The Histone Methyltransferase Ezh2 Controls Mechanisms of Adaptive Resistance to Tumor Immunotherapy

Zingg, Daniel; Arenas-Ramirez, Natalia; Sahin, Dilara; Rosalia, Rodney A; Antunes, Ana T; Haeusel, Jessica; Sommer, Lukas; Boyman, Onur

DOI: https://doi.org/10.1016/j.celrep.2017.07.007

Article

Cell Reports

The Histone Methyltransferase Ezh2 Controls Mechanisms of Adaptive Resistance to Tumor Immunotherapy

Graphical Abstract

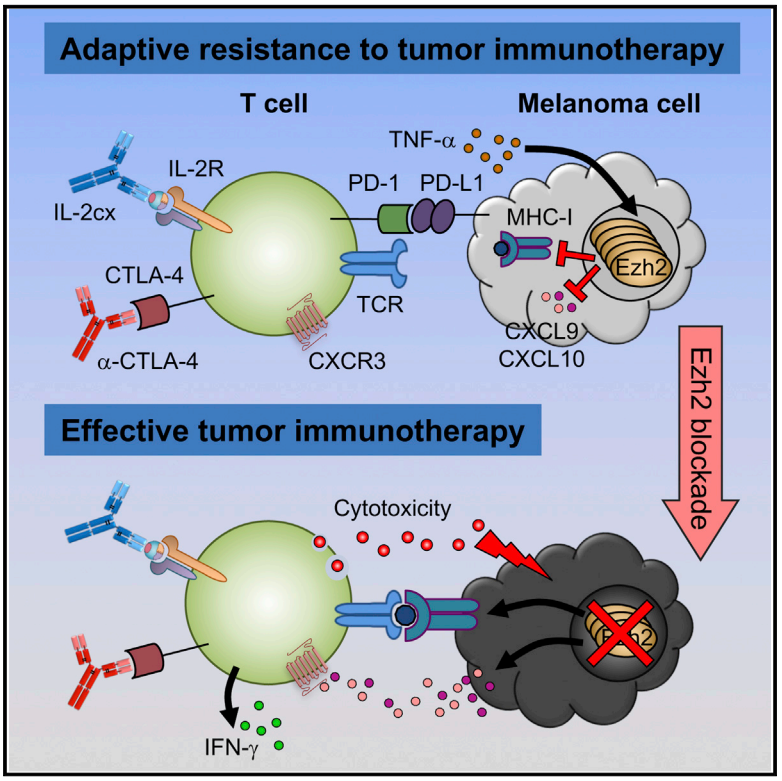

Highlights

- Intratumoral T cells and TNF-α cause Ezh2 upregulation in melanoma cells
- Ezh2 silences immunogenicity and antigen presentation in melanoma
- Ezh2 blockade reverses melanoma resistance mechanisms
- Ezh2 inactivation synergizes with anti-CTLA-4 and IL-2 immunotherapy

Authors

Daniel Zingg, Natalia Arenas-Ramirez, Dilara Sahin, ..., Jessica Haeusel, Lukas Sommer, Onur Boyman

Correspondence

lukas.sommer@anatom.uzh.ch (L.S.), onur.boyman@uzh.ch (O.B.)

In Brief

Zingg et al. investigate the mechanisms of adaptive resistance to tumor immunotherapy. They find that intratumoral TNF-α production and T cell accumulation promote Ezh2 upregulation in melanoma cells, resulting in loss of immunogenicity and antigen presentation. Ezh2 inactivation reverses these effects and synergizes with anti-CTLA-4 and IL-2 immunotherapies.

Zingg et al., 2017, Cell Reports *20*, 854–867
July 25, 2017
http://dx.doi.org/10.1016/j.celrep.2017.07.007

CellPress

OPEN ACCESS
CellPress

Cell Reports
Article

The Histone Methyltransferase Ezh2 Controls Mechanisms of Adaptive Resistance to Tumor Immunotherapy

Daniel Zingg,[1,3] Natalia Arenas-Ramirez,[2,3] Dilara Sahin,[2] Rodney A. Rosalia,[2] Ana T. Antunes,[1] Jessica Haeusel,[1] Lukas Sommer,[1,4,*] and Onur Boyman[2,4,5,*]

[1]Stem Cell Biology, Institute of Anatomy, University of Zurich, 8057 Zurich, Switzerland
[2]Department of Immunology, University Hospital Zurich, University of Zurich, 8091 Zurich, Switzerland
[3]These authors contributed equally
[4]Senior author
[5]Lead Contact
*Correspondence: lukas.sommer@anatom.uzh.ch (L.S.), onur.boyman@uzh.ch (O.B.)
http://dx.doi.org/10.1016/j.celrep.2017.07.007

SUMMARY

Immunotherapy and particularly immune checkpoint inhibitors have resulted in remarkable clinical responses in patients with immunogenic tumors, although most cancers develop resistance to immunotherapy. The molecular mechanisms of tumor resistance to immunotherapy remain poorly understood. We now show that induction of the histone methyltransferase Ezh2 controls several tumor cell-intrinsic and extrinsic resistance mechanisms. Notably, T cell infiltration selectively correlated with high EZH2-PRC2 complex activity in human skin cutaneous melanoma. During anti-CTLA-4 or IL-2 immunotherapy in mice, intratumoral tumor necrosis factor-α (TNF-α) production and T cell accumulation resulted in increased Ezh2 expression in melanoma cells, which in turn silenced their own immunogenicity and antigen presentation. Ezh2 inactivation reversed this resistance and synergized with anti-CTLA-4 and IL-2 immunotherapy to suppress melanoma growth. These anti-tumor effects depended on intratumorally accumulating interferon-γ (IFN-γ)-producing PD-1^{low} CD8$^+$ T cells and PD-L1 downregulation on melanoma cells. Hence, Ezh2 serves as a molecular switch controlling melanoma escape during T cell-targeting immunotherapies.

INTRODUCTION

The immune system plays a dual role during cancer elimination versus progression. Immune cells recognize and eliminate malignant cells via a process termed cancer immunosurveillance, which relies on interferon-γ (IFN-γ) and tumor necrosis factor α (TNF-α) production by CD4$^+$ and CD8$^+$ T cells (Schreiber et al., 2011). However, these immune mechanisms also pressurize tumor cells to initiate a dedifferentiation program associated with loss of dominant tumor antigens and silencing of the antigen-processing and presenting machinery (Hölzel and Tüting, 2016; Schreiber et al., 2011). In addition to these cell-intrinsic modifications, extrinsic signals can contribute to cancer cell resistance. Thus, various factors are able to promote an immunosuppressive tumor microenvironment, including certain cytokines, chemokines, enzymes, and negative costimulatory molecules, as well as CD4$^+$ CD25$^+$ forkhead boxP3 (FoxP3)$^+$ regulatory T (Treg) cells and CD11b$^+$ Gr-1$^+$ myeloid-derived suppressor cells (MDSCs).

Anti-tumor effector T cells facing antigen persistence upregulate PD-1 and become exhausted when encountering PD-L1-expressing tumor cells, thus progressively losing their effector functions, including IFN-γ production (Wherry and Kurachi, 2015). Accordingly, immune checkpoint molecules, including PD-1 and its ligand, PD-L1, contribute to an immunosuppressive tumor microenvironment (Schreiber et al., 2011; Topalian et al., 2015; Tumeh et al., 2014). Therapies targeting PD-1, PD-L1, and CTLA-4, also termed immune checkpoint inhibitors, increase the anti-tumor T cell response and have shown some considerable anti-tumor effects in patients with metastatic cancer, particularly melanoma (Larkin et al., 2015; Topalian et al., 2015). However, despite these treatments, many cancer patients experience progression of their disease, probably indicating that tumor cells resort to resistance strategies when facing heightened immune pressure. The molecular pathways determining tumor escape from immunotherapy remain poorly understood.

To study the molecular mechanisms of resistance to anti-cancer treatment, we chose to use two different modes of immunotherapy in three mouse models of melanoma. Interleukin-2 (IL-2) immunotherapy is approved for metastatic melanoma (Rosenberg, 2014) and has the advantage of stimulating anti-cancer T cell responses independently of PD-1, PD-L1, and CTLA-4 expression. We and others have been studying IL-2 and improved IL-2 formulations, including IL-2/anti-IL-2 monoclonal antibody (mAb) complexes (IL-2cx), in various preclinical and clinical settings of metastatic melanoma (Arenas-Ramirez et al., 2015). In preclinical studies, IL-2cx, but not free IL-2 or anti-IL-2 mAb (Boyman et al., 2006), exerted vigorous anti-tumor immune responses against syngeneic B16-F10 melanoma and other cancers in mice (Arenas-Ramirez et al., 2016; Krieg et al.,

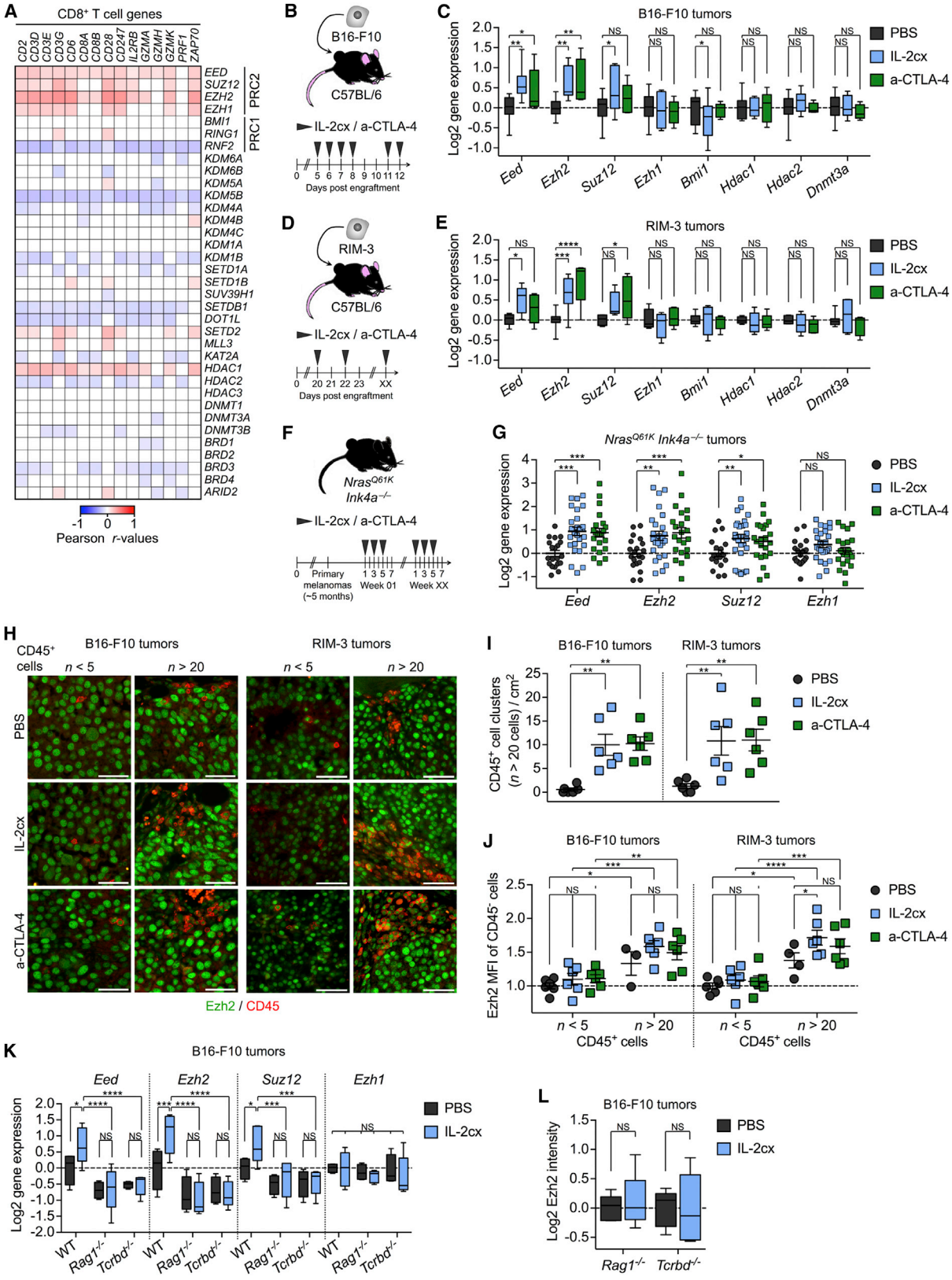

(legend on next page)

2010; Levin et al., 2012). However, despite continuous treatment with IL-2cx, B16-F10 melanoma nodules ultimately grew out in most animals, suggesting subversion of immune-mediated tumor control.

In human melanoma, genetic determinants of immune resistance remain elusive, whereas transcriptomic alterations appear to be a major feature of immune evasion (Hugo et al., 2016; Van Allen et al., 2015). We thus hypothesized that immune pressure-induced epigenetic rewiring of the transcriptional landscape might drive immune resistance in melanoma cells. The polycomb repressive complex 2 (PRC2) is a prominent chromatin-remodeling complex that mediates transcriptional repression via trimethylation of lysine 27 in histone 3 (H3K27me3). PRC2 consists of embryonic ectoderm development (EED), suppressor of zeste 12 (SUZ12), and the histone methyltransferase unit EZH2, among others (Kim and Roberts, 2016). Here, we show that Ezh2 controls crucial melanoma cell-intrinsic and extrinsic mechanisms of immune resistance to immunotherapy.

RESULTS

T Cell Infiltrates Correlate with PRC2 Subunit Upregulation in Melanoma

Comparison of $CD8^+$ T cell-associated genes (Bindea et al., 2013) with epigenetic modifier genes within The Cancer Genome Atlas (TCGA) human skin cutaneous melanoma (SKCM) RNA-sequencing (RNA-seq) data (Cancer Genome Atlas Network, 2015) revealed a strong positive correlation of $CD8^+$ T cell genes with PRC2 complex members *EED*, *SUZ12*, *EZH2*, and *EZH1*, as well as with *HDAC1* and *SETD2* (Figure 1A). Conversely, PRC1 members and all other tested epigenetic modifier genes did not correlate positively with $CD8^+$ T cell genes. These data suggested that intratumoral $CD8^+$ T cell accumulation might promote PRC2 upregulation in melanoma.

To functionally investigate this hypothesis, we used two transplantable and one spontaneous melanoma model. (1) The highly proliferative B16-F10 murine melanoma cell line becomes visible and palpable 3–4 days after cutaneous injection to syngeneic C57BL/6 wild-type (WT) mice, and, after day 4, is difficult to control by IL-2cx immunotherapy or immune checkpoint inhibitors (Arenas-Ramirez et al., 2016; Krieg et al., 2010; Ueha et al., 2015). (2) RIM-3 melanoma cells are derived from a primary tumor from *Tyr::Nras*^{Q61K} *Cdkn2a (p16*^{Ink4a}*)*-deficient (hereafter termed *Nras*^{Q61K} *Ink4a*$^{-/-}$) transgenic mice on a C57BL/6 background and display slower growth kinetics than B16-F10 upon transplantation (Zingg et al., 2015). (3) *Nras*^{Q61K} *Ink4a*$^{-/-}$ mice spontaneously develop primary skin melanomas at 5–7 months of age (Shakhova et al., 2012; Zingg et al., 2015). Similar to B16-F10, IL-2cx delays but does not prevent melanoma in *Nras*^{Q61K} *Ink4a*$^{-/-}$ animals (Arenas-Ramirez et al., 2016).

In all three melanoma models, immunotherapy by IL-2cx or anti-CTLA-4 mAb caused an increase in mRNA expression of the PRC2 members *Eed*, *Ezh2*, and *Suz12* (Figures 1B–1G). In contrast, expression of *Ezh1* and further key epigenetic modifiers were not changed by immunotherapy. Notably, in B16-F10 and RIM-3 tumor areas infiltrated by $CD45^+$ leukocytes, higher Ezh2 levels were found in comparison to areas with little immune cell infiltrates (Figures 1H–1J), in agreement with the TCGA-SKCM data (Figure 1A).

In comparison to WT mice, in animals deficient in recombinase-activating gene 1 (*Rag1*$^{-/-}$; thus devoid of T and B cells) or in mice lacking both T cell receptor (TCR) $\alpha\beta^+$ and TCR$\gamma\delta^+$ T cells (*Tcrbd*$^{-/-}$), IL-2cx immunotherapy failed to upregulate PRC2, particularly Ezh2, at the mRNA and protein levels (Figures 1K, 1L, S1A, and S1B). Moreover, IL-2cx or anti-CTLA-4 treatment of B16-F10 or RIM-3 cells in vitro did not cause any significant upregulation of PRC2 (Figure S1C). Together, these data suggest that tumor-infiltrating T cells promote PRC2 upregulation in both human and mouse melanoma.

Ezh2 Promotes Melanoma Dedifferentiation and Loss of Immunogenicity

We next investigated whether immunotherapy-induced increase in Ezh2 resulted in enhanced Ezh2 activity. Indeed, IL-2cx or anti-CTLA-4 immunotherapy resulted in increased Ezh2 protein levels in B16-F10 and RIM-3 melanomas, which was accompanied by a global increase in H3K27me3 (Figures 2A–2C and S2A–S2E). Of note, upon immunotherapy, H3K27me3 levels did not increase in B16-F10 tumors from *Rag1*$^{-/-}$ or *Tcrbd*$^{-/-}$ mice (Figures S1A and S1B). To study the molecular consequences of enhanced Ezh2 activity in melanoma cells, we sought to identify potential Ezh2 target genes (ETGs) associated with tumor cell immunogenicity. Immunotherapy of B16-F10 or RIM-3-harboring animals led to transcriptional silencing of a variety of

Figure 1. Intratumoral T Cells Correlate with PRC2 Upregulation in Melanoma

(A) Heatmap showing Pearson's product-moment correlation coefficients (*r*) for the expression of $CD8^+$ T cell signature versus epigenetic modifier genes, based on TCGA-SKCM RNA-seq data (n = 470). Colored squares indicate $p < 0.05$.

(B–G) qRT-PCR for epigenetic modifier genes in melanoma nodules to assess effects of IL-2/anti-IL-2 antibody complex (IL-2cx) or anti-CTLA-4 (a-CTLA-4) immunotherapy in mice harboring B16-F10 (B and C) or RIM-3 (D and E) or in *Nras*^{Q61K} *Ink4a*$^{-/-}$ mice (F and G). Data are presented as median ± 100% range of n = 11 (C, PBS), n = 6 (C and E, IL-2cx), n = 5 (C and E, a-CTLA-4), or n = 7 (E, PBS) or mean ± SEM of n = 20 tumors of eight mice (G, PBS), n = 26 tumors of nine mice (G, IL-2cx), and n = 22 tumors of ten mice (G, a-CTLA-4) from three (C and E) independent experiments or one experiment (G).

(H–J) Immunofluorescence staining for Ezh2 and CD45 in B16-F10 and RIM-3 melanoma nodules from PBS-, IL-2cx-, and a-CTLA-4-treated mice (H) to quantify areas poor or rich in $CD45^+$ cells ($CD45^+$ n < 5 versus n > 20/field; I) and Ezh2 mean fluorescence intensity (MFI) of $CD45^-$ cells (J). Scale bars, 50 μm. Data are presented as mean ± SEM of n = 6 from three independent experiments.

(K) qRT-PCR for PRC2 genes on B16-F10 melanoma nodules from WT, *Rag1*$^{-/-}$, or *Tcrbd*$^{-/-}$ mice receiving PBS or IL-2cx. Data are presented as median ± 100% range of n = 4 (PBS) and n = 5 (IL-2cx) from two independent experiments.

(L) Quantification of Ezh2 from western blots (Figure S1A) on B16-F10 melanoma nodules from *Rag1*$^{-/-}$ or *Tcrbd*$^{-/-}$ mice receiving PBS or IL-2cx. Data are presented as median ± 100% range of n = 5 from two independent experiments.

p values were calculated using ANOVA and Fisher's least significant difference (LSD) (C–K) or unpaired Student's t tests (L). NS, not significant; *p < 0.05; **p < 0.01; ***p < 0.001; ****p < 0.0001. See also Figure S1.

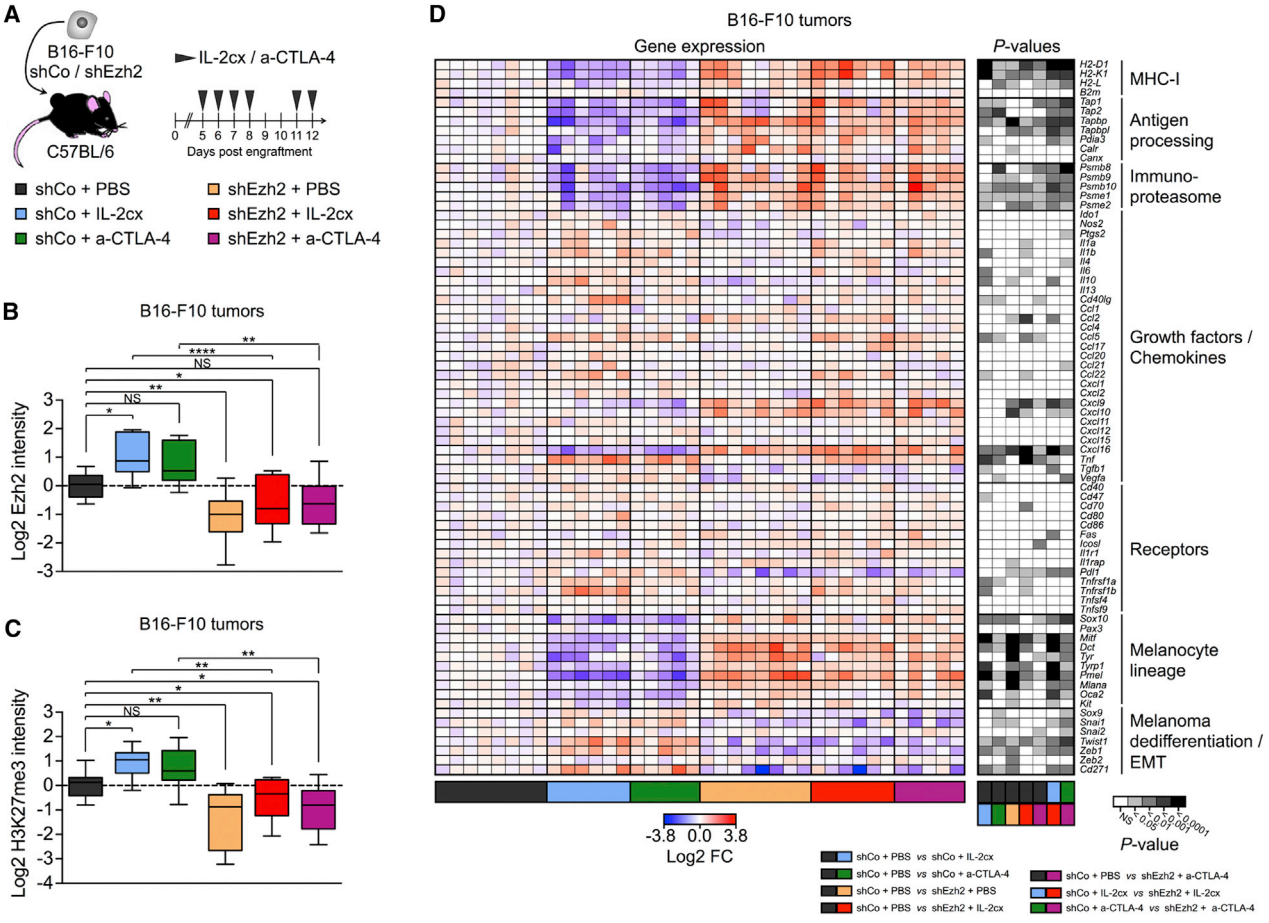

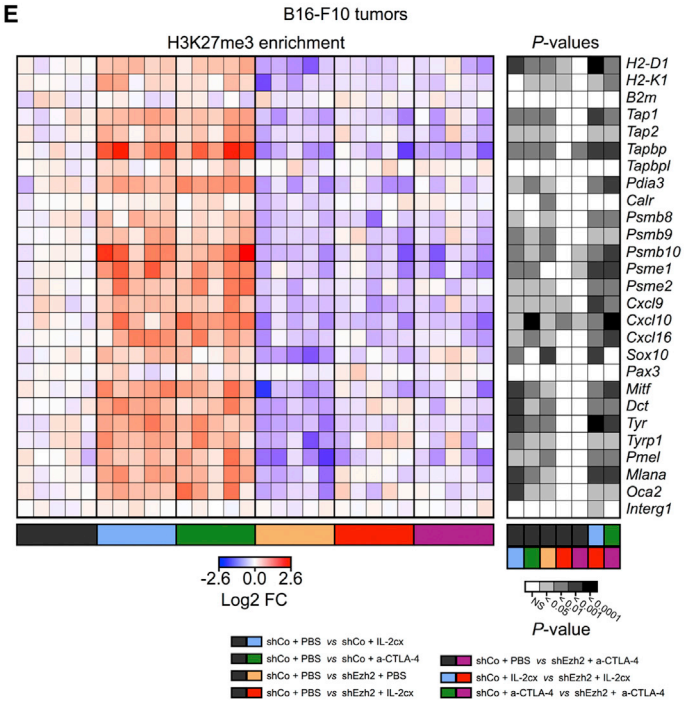

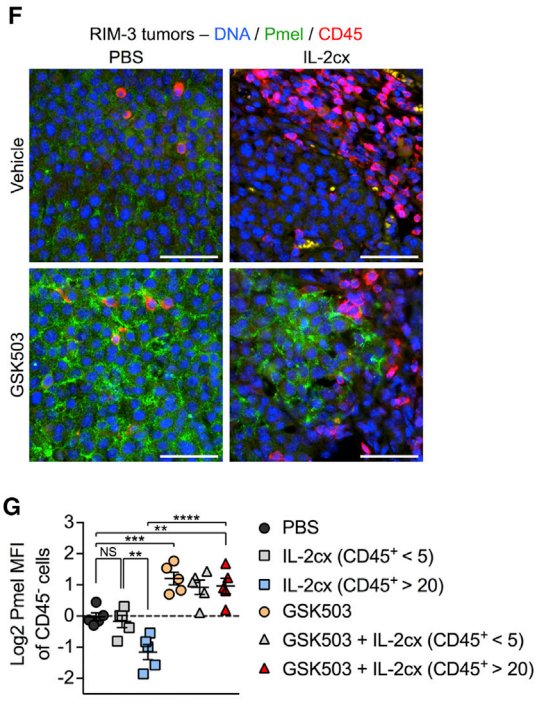

(legend on next page)

genes, including members of major histocompatibility complex class I (MHC-I) molecules, antigen processing machinery, immunoproteasome, and several chemokines (Figures 2D and S2F). Furthermore, a set of melanocyte lineage genes (Denecker et al., 2014; Shakhova et al., 2012) was downregulated, some of which constitute known melanoma antigens (*Dct* and *Pmel*, also known as Trp2 and gp100). In contrast, expression of genes previously connected to melanoma dedifferentiation and epithelial-mesenchymal transition (EMT) (Caramel et al., 2013; Hölzel and Tüting, 2016; Shakhova et al., 2012) substantially increased upon immunotherapy (Figures 2D and S2F). Next, we addressed whether transcriptionally silenced genes were direct Ezh2 targets by performing chromatin immunoprecipitation (ChIP) for Ezh2 and H3K27me3. Indeed, in many of the promoter regions of silenced genes, we detected enrichment for Ezh2 and H3K27me3 upon immunotherapies (Figures 2E, S2G, and S2H). Importantly, changes in gene expression were most apparent in tumor areas rich in immune cell infiltrates, as exemplified by Pmel and Mitf downregulation and Zeb1 upregulation (Figures 2F, 2G, and S3A–S3D).

Ezh2 Inactivation Restores Melanoma Immunogenicity

To demonstrate that immunotherapy-induced gene expression changes were dependent on Ezh2, we inhibited Ezh2 function using either a short hairpin RNA against *Ezh2* (shEzh2) or GSK503, a specific chemical inhibitor of Ezh2 (Béguelin et al., 2013). RNAi by shEzh2 effectively reduced Ezh2 levels in vivo and in vitro (Figures 2B, S2A, and S2B), while both RNAi and GSK503 led to a considerable loss of H3K27me3 in melanoma samples, even in animals receiving immunotherapy (Figures 2C and S2A–S2E). Importantly, upon *Ezh2* silencing, loss of Ezh2 and H3K27me3 was observed specifically in promoter regions of aforementioned ETGs downregulated upon immunotherapy (Figures 2E, S2G, and S2H). Accordingly, Ezh2 inactivation in B16-F10 and RIM-3 promoted upregulation of these ETGs, which was accompanied by suppression of dedifferentiation genes (Figures 2D and S2F). This was most conspicuous for tumor areas rich in $CD45^+$ immune cell infiltrates (Figures 2F, 2G, and S3A–S3D).

Ezh2 Inactivation Synergizes with Anti-melanoma Immunotherapy

Our data suggested that Ezh2 inactivation was sufficient to reverse immunotherapy-induced immune resistance in melanoma. Indeed, compared to their monotherapies, a combination of IL-2cx and *Ezh2* RNAi or anti-CTLA-4 and *Ezh2* RNAi significantly delayed tumor growth, reducing tumor volume by over 75% (Figures 3A–3C). Similar effects were observed in mice harboring B16-F10 following administration of GSK503 combined with immunotherapy (Figures 3D–3F). Strikingly, co-administration of GSK503 and immunotherapy was also very efficient in $Nras^{Q61K}$ $Ink4a^{-/-}$ animals when treated at developing primary melanomas (Figure 3G). While the monotherapies showed some anti-tumor effects over PBS, the combination treatments were highly efficient in causing melanoma regression (Figure 3H). Consequently, at the time point of sacrifice, skin melanoma volumes and counts in mice receiving combination therapies were significantly reduced in comparison to monotherapies (Figures 3H, 3I, and S3E), resulting in prolonged skin-melanoma-specific survival (Figure 3J). However, in mice with LLC1 Lewis lung carcinoma or MC-38 murine colon carcinoma, GSK503 + IL-2cx did not provide any advantage over IL-2cx (Figures S3F and S3G), which correlated with the tumors' weak or absent upregulation of PRC2 members (Figure S3H).

Combination Therapy Stimulates $CD8^+$ T Cells and Suppresses the PD-1/PD-L1 Axis

To assess the mechanism of action of immunotherapy combined with Ezh2 inhibition, we analyzed tumor-infiltrating lymphocytes (TILs) in comparison to lymphocytes in tumor-draining lymph nodes (TDLNs). Compared to control or GSK503 alone, immunotherapy, more notably GSK503 + IL-2cx immunotherapy, led to increased $CD8^+$ T cell counts in TILs and TDLNs (Figures 4A and 4B). The difference in $CD8^+$ TILs between IL-2cx and GSK503 + IL-2cx was not due to increased systemic proliferation and accumulation of $CD8^+$ T cells during GSK503 + IL-2cx immunotherapy (Figures S4A and S4B). Although percentages of $CD4^+$ $CD25^+$ $FoxP3^+$ Treg cells were increased in TDLNs, Treg cell counts in TDLNs and TILs were not significantly different between treatment groups (Figures 4A and 4B). This resulted in a ratio of $CD8^+$ T cells to Treg cells of 15 in TILs and 13 in TDLNs for GSK503 + IL-2cx immunotherapy, hence favoring intratumoral $CD8^+$ T cells with combination therapy (Figure 4C). Contrarily, total $CD4^+$ T cells, natural killer (NK) cells, MHC-II^+ B and antigen-presenting cells, and $CD11b^+$ $Gr\text{-}1^+$ MDSCs were not significantly changed in TILs upon treatment, although some differences were noted in TDLNs (Figures 4A, 4B, and S4C–S4H). Similar effects on $CD8^+$ T and Treg cells were obtained using shEzh2 B16-F10 instead of GSK503 or with anti-CTLA-4 immunotherapy instead of IL-2cx (Figures S5A–S5D).

Phenotypic and functional analysis of TILs demonstrated that $CD8^+$ T cells in animals receiving GSK503 + IL-2cx were mainly

Figure 2. Ezh2 Promotes Melanoma Dedifferentiation and Loss of Immunogenicity

(A) Graphical representation of model system and color-coding of experimental groups, including mice receiving shCo- or shEzh2-transfected B16-F10 melanoma cells followed by PBS, IL-2cx, or a-CTLA-4.

(B and C) Quantification of western blots (Figure S2A) for Ezh2 (B) and H3K27me3 (C) on B16-F10 from animals treated as in (A).

(D and E) qRT-PCR for genes relevant for tumor-immune interaction (D) and ChIP for H3K27me3 and subsequent qPCR in promoter regions of selected loci (E) on B16-F10 from animals treated as in (A). Heatmaps show log2 fold change (FC) values relative to average of controls (shCo + PBS) and p values from comparisons of individual groups as indicated by color-coding.

(F and G) Immunofluorescence staining for Pmel and CD45 on RIM-3 following PBS, IL-2cx, GSK503, or GSK503 + IL-2cx (F) to quantify Pmel MFI of $CD45^-$ cells in areas poor or rich in $CD45^+$ cells ($CD45^+$ $n < 5$ versus $n > 20$/field, G). Scale bars, 50 μm.

Data are presented as median ± 100% range of n = 7–10 (B and C), as individual values of n = 5–8 (D) and n = 5 (E), and as mean ± SEM of n = 5 (G) from three (B–E) or two (G) independent experiments. p values were calculated using ANOVA and the Fisher's LSD test. NS, not significant; *$p < 0.05$; **$p < 0.01$, ***$p < 0.001$; ****$p < 0.0001$. See also Figures S2 and S3.

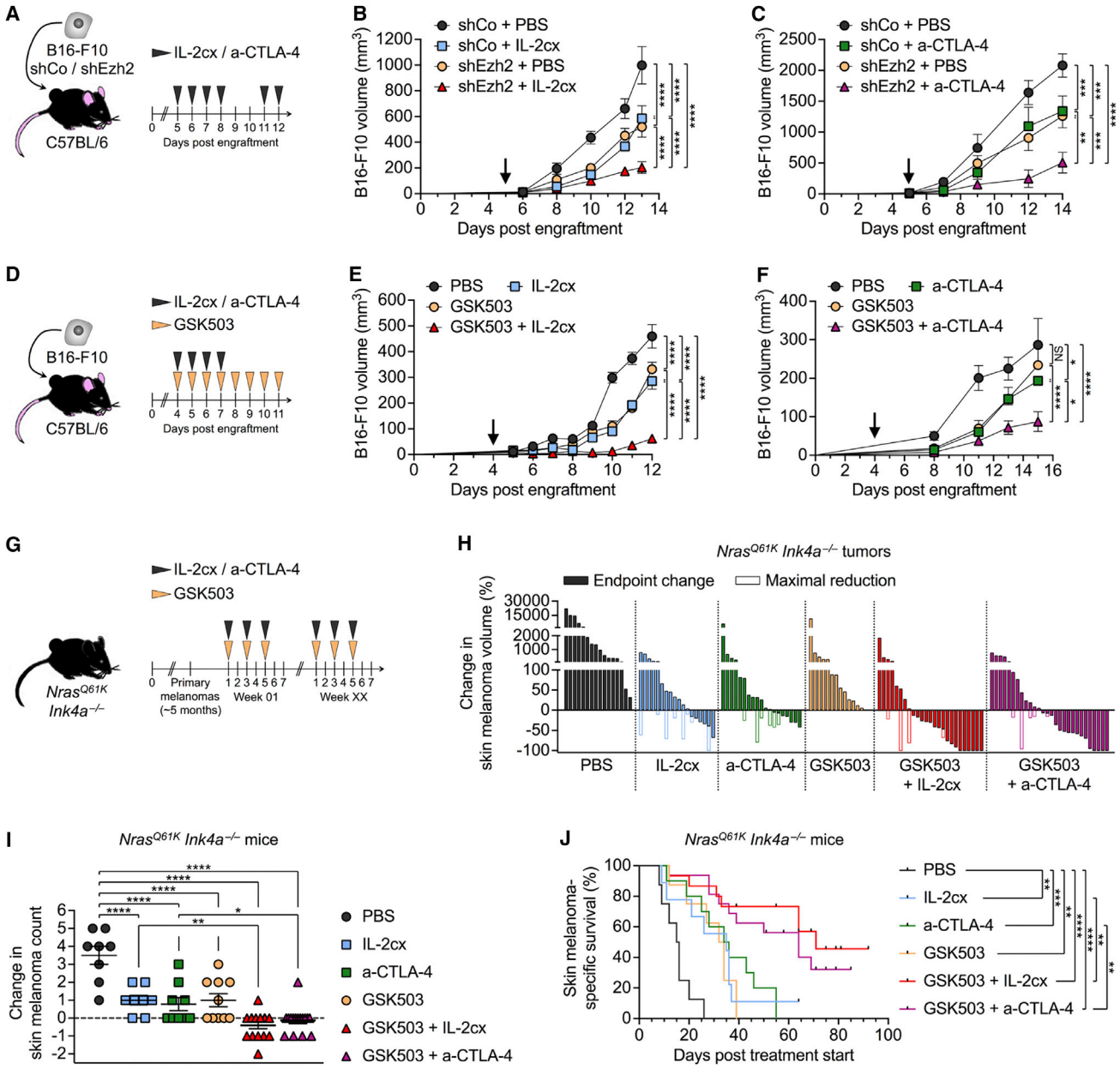

Figure 3. Ezh2 Inactivation Synergizes with Anti-melanoma Immunotherapy

(A–F) Tumor growth kinetics in mice harboring shCo- or shEzh2-transfected B16-F10 (A–C) or WT B16-F10 (D–F), and receiving treatments as indicated in (A) and (D). Black arrows mark the time point when treatment started. Data are presented as mean ± SEM of n = 15 (B), n = 5 (C), n = 25 (E), and n = 4–6 (F) from three (B), six (E), and two (F) independent experiments or one experiment (C).

(G and H) Maximal volume reduction and volume at the time point of sacrifice of individual skin melanomas in *Nras*^{Q61K} *Ink4a*$^{-/-}$ transgenic mice (H) from animals treated as in (G). Data are presented as individual values for n = 17 tumors from eight mice (PBS), n = 18 tumors from nine mice (IL-2cx), n = 19 tumors from ten mice (a-CTLA-4), n = 15 tumors from eight mice (GSK503), n = 25 tumors from 15 mice (GSK503 + IL-2cx), and n = 28 tumors from 16 mice (GSK503+ a-CTLA-4) from one experiment.

(I) Change in skin melanoma counts (treatment start versus endpoint) of individual *Nras*^{Q61K} *Ink4a*$^{-/-}$ mice. Treatments as in (G). Data are represented as mean ± SEM.

(J) Kaplan-Meier curves comparing melanoma-specific survival of *Nras*^{Q61K} *Ink4a*$^{-/-}$ mice. Treatments as in (G).

p values were calculated using ANOVA and Fisher's LSD (B–I) or log-rank (Mantel-Cox) tests (J). NS, not significant; *p < 0.05; **p < 0.01; ***p < 0.001; ****p < 0.0001. See also Figure S3.

CD44^{high} CD62L^{variable} CD69^{low} with low expression of PD-1 and of other immune checkpoint molecules, such as T cell immunoglobulin and mucin domain-3 (TIM-3) and lymphocyte activation gene-3 (LAG-3) (Figures 4D, 4E, S5E, and S5F). This suggested Ezh2 inhibition plus IL-2cx immunotherapy prevented intratumoral accumulation of exhausted CD8$^+$ T cells.

Furthermore, immunotherapy promoted PD-L1 upregulation in melanomas (Figures 4F, 4G, and S5G). Thus, Pax3$^+$ melanoma cells increased PD-L1 upon IL-2cx treatment, particularly in areas rich in CD3$^+$ TILs (Figures 4F and 4G). This was consistent with the observed increase of Zeb1 upon immunotherapy (Figures S3C and S3D), which has been shown to enhance PD-L1 expression (Chen et al., 2014). Ezh2 inactivation, however, led to reduced PD-L1 mRNA levels and a decrease in PD-L1$^+$ Pax3$^+$ melanoma cells, which was maintained during concomitant IL-2cx or anti-CTLA-4 immunotherapy (Figures 4F, 4G, S5G, and S5H). Downregulation of the immunosuppressive PD-1/PD-L1 axis by Ezh2 blockade plus IL-2cx combination therapy was remarkably efficient, even when treatment was initiated only after formation of visible tumor nodules, while addition of a blocking anti-PD-1 mAb was unable to further improve the anti-tumor effects of GSK503 (Figure 4H). Thus, immunotherapy combined with Ezh2 blockade results in the accumulation of non-exhausted effector CD8$^+$ T cells within TILs and inhibition of the PD-1/PD-L1 axis.

Combination Immunotherapy Depends on Migrating IFN-γ$^+$ CD8$^+$ T Cells

The demonstration in animals receiving Ezh2 inhibitor plus immunotherapy that CD8$^+$ T cells predominated TILs and expressed low PD-1 levels suggested that tumor control depended on these cells. We thus compared combination therapy using GSK503 + IL-2cx in WT animals versus *Rag1*$^{-/-}$ or *Tcrbd*$^{-/-}$ mice that lack T cells (and also B cells in the case of *Rag1*$^{-/-}$) but harbor functional NK cells. The anti-melanoma effect of combination therapy was lost in both *Tcrbd*$^{-/-}$ and *Rag1*$^{-/-}$ mice (Figure 5A), thus demonstrating that T cells, but not B or NK cells, exerted the tumoricidal effects. Further experiments using specific depleting mAbs showed that CD8$^+$, but not CD4$^+$ T cells, played a crucial role in the anti-tumor response. Thus, during GSK503 + IL-2cx treatment, tumor control was lost in animals injected with anti-CD8 mAb, while mice receiving anti-CD4 mAb were able to suppress tumor growth (Figure 5B).

The anti-tumor effect of GSK503 + IL-2cx depended on IFN-γ production, as demonstrated using *Ifng*$^{-/-}$ mice (Figure 5C). In line with these data, high numbers of both CD90.1$^-$ polyclonal CD8$^+$ (Figure 5D) and, upon adoptive transfer, CD90.1$^+$ Pmel-specific TCR-transgenic CD8$^+$ T cells (Figure 5E) produced IFN-γ when isolated from TDLNs of mice receiving IL-2cx or GSK503 + IL-2cx combination therapy, whereas IFN-γ-producing cells were significantly lower in the other groups (Figures 5D and 5E). Also, ex vivo cytotoxic activity of CD8$^+$ T cells, as assessed by using the degranulation marker CD107a, was highest following combination immunotherapy, as shown by higher numbers of CD107a$^+$ CD8$^+$ T cells within TILs from animals treated with Ezh2 blockade plus IL-2cx (Figure 5F).

In line with our observation that Ezh2 inactivation plus immunotherapy favored intratumoral accumulation of CD8$^+$ T cells rather than their proliferation systemically or in TDLNs (Figures 4B, S4A, and S5I), intratumoral expression of the T cell-attractant chemokines Cxcl9 and Cxcl10 increased upon Ezh2 inactivation (Figure 5G). In contrast, monoimmunotherapies resulted in PRC2-mediated silencing of *Cxcl9* and *Cxcl10* (Figures 2D, 2E, 5G, S2F, and S2H). Accordingly, targeting of CXCR3, the receptor of the aforementioned chemokines, significantly reduced the anti-tumor effect of GSK503 + IL-2cx (Figure 5H).

TNF-α-Producing T Cells Cause PRC2-Mediated Melanoma Immune Resistance

Based on our findings, we reasoned that soluble factors released by the immune infiltrate might promote PRC2 gain of function in melanoma. To test this hypothesis, we applied a panel of growth factors and chemokines to B16-F10 and RIM-3 in vitro cultures. This screen revealed TNF-α to be the strongest factor in inducing upregulation of PRC2 subunits, whereas other prototypic pro-inflammatory cytokines only minimally upregulated or, in the case of IFN-γ, even downregulated PRC2 members (Figure 6A). In contrast to IFN-γ, inflammation and particularly production of TNF-α have previously been shown to promote melanoma dedifferentiation and tumor immune escape (Hölzel and Tüting, 2016). Thus, we further investigated the relevance of TNF-α in PRC2-dependent melanoma immune evasion. TNF-α stimulation of B16-F10 cells induced Ezh2 expression and, consequently, led to increased H3K27me3 levels (Figures 6B, 6C, and S6A). Moreover, exposure of B16-F10 and RIM-3 cells to TNF-α resulted in silencing of several antigen processing, presentation, and melanocyte lineage genes, as well as *Cxcl9* and *Cxcl10*, in an Ezh2-dependent fashion (Figures 6D and S6B). This process inversely correlated with enrichment of H3K27me3 in the promoter regions of these genes (Figures 6E and S6C).

The TNF-α- and Ezh2-dependent transcriptional changes appeared comparable to the gene expression changes observed in tumors upon immunotherapies (Figures 2 and S2). Interestingly, B16-F10 and RIM-3 tumor lysates showed increased expression of *Tnf* mRNA and TNF-α protein when derived from animals receiving immunotherapy (Figures 6F and 6G). Similarly, *Tnf* expression was increased in tumors from *Nras*^{Q61K} *Ink4a*$^{-/-}$ mice treated with immunotherapy (Figure 6H). *Tnf* expression and TNF-α concentration in tumor nodules depended on the presence of T cells, as demonstrated using *Rag1*$^{-/-}$ and *Tcrbd*$^{-/-}$ mice (Figures 6I and 6J). Furthermore, *Tnf* transcripts were nearly absent in B16-F10 tumors from *Tnf*$^{-/-}$ animals, suggesting that TNF-α was mostly released by host-derived cells rather than tumor cells (Figure 6K). Importantly, IL-2cx immunotherapy failed to upregulate PRC2 subunits, including Ezh2, in *Tnf*$^{-/-}$ mice (Figure 6L).

DISCUSSION

To better understand tumor resistance to immunotherapy, we investigated the role of the epigenetic modifier Ezh2 during anti-CTLA-4 and IL-2 treatment in models of aggressive melanoma. Our data demonstrate that immunotherapy led to increased Ezh2 activity that was dependent on T cells and TNF-α, resulting in melanoma dedifferentiation, loss of immunogenicity, and upregulation of the PD-1/PD-L1 axis. These

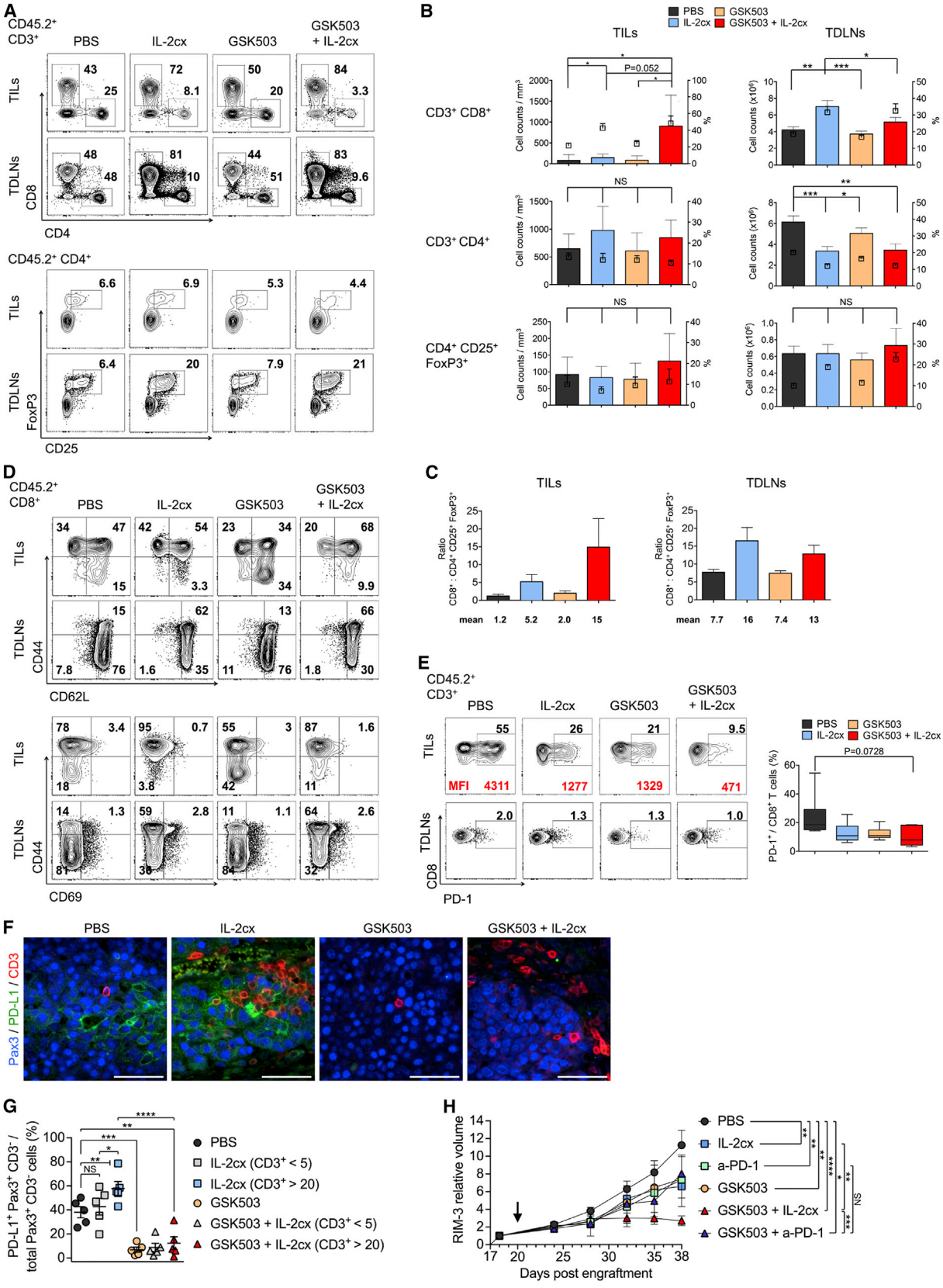

(legend on next page)

findings fit and extend previous reports of immunotherapy using adoptive T cell transfer or activating T cells resulting in TNF-α-dependent melanoma dedifferentiation and PD-L1 upregulation (Hölzel and Tüting, 2016; Spranger et al., 2013). Moreover, increased expression of the melanoma dedifferentiation gene *Zeb1*, as seen here upon immunotherapy, has been associated with enhanced PD-L1 expression (Chen et al., 2014; Wang et al., 2014).

However, these changes proved to be dynamic and malleable, in that inhibition of Ezh2 restored presentation of several dominant melanoma antigens while downregulating PD-L1 on melanoma cells. In parallel, PD-1 expression on tumor-antigen-specific and polyclonal melanoma-infiltrating $CD8^+$ T cells decreased significantly, thus improving effector functions of the cells, including IFN-γ production and cytotoxicity. The net result of these effects was control of melanoma growth and, in the case of $Nras^{Q61K}$ $Ink4a^{-/-}$ mice, tumor regression, which clearly exceeded the efficacy of monotherapies consisting of IL-2cx, anti-CTLA-4, or Ezh2 inhibition (Arenas-Ramirez et al., 2016; Krieg et al., 2010; Ueha et al., 2015; Zingg et al., 2015). Unlike melanoma, mice carrying LLC1 Lewis lung carcinoma or MC-38 murine colon carcinoma showed barely any upregulation of Ezh2 upon immunotherapy. Consequently, these cancer models did not benefit from the addition of Ezh2 blockade to immunotherapy, pointing to a melanoma-specific role of PRC2 in governing immune evasion.

Recent reports suggested a somewhat antagonistic role of PRC2 in the anti-tumor immune response (Peng et al., 2015; Zhao et al., 2016). In ovarian and colon cancer cells, PRC2 was able to repress $CD8^+$ T cell trafficking to the tumor site (Nagarsheth et al., 2016; Peng et al., 2015). Consistent with these data we found that upon Ezh2 inactivation, effector $CD8^+$ T cells preferentially accumulated intratumorally in a CXCL9/CXCL10-CXCR3-dependent fashion. Moreover, we complement these findings by demonstrating that T cell- and TNF-α-dependent Ezh2 upregulation is implicated in several other immune escape mechanisms, namely melanoma dedifferentiation, tumor cell immunogenicity, and the PD-1/PD-L1 axis. Thus, Ezh2 inactivation locks melanoma cells in an immunogenic state and facilitates efficient $CD8^+$ T cell-mediated anti-tumor responses during immunotherapy. However, Ezh2 has also been shown to affect T cells directly by improving survival and activity of anti-tumor $CD8^+$ T cells (Zhao et al., 2016) and maintaining $Foxp3^+$ Treg cells (DuPage et al., 2015). In our study, however, melanoma cell-specific *Ezh2* RNAi led to similar effects as systemic Ezh2 blockade. Furthermore, despite systemic Ezh2 inhibition, we did not find any evidence for compromised $CD8^+$ T cell function in our melanoma models, while $Foxp3^+$ Treg cells failed to accumulate within TILs. Hence, this discrepancy might be due to the tumor models or immunotherapies used in the different studies.

High EZH2 expression is associated with unfavorable prognosis in human cutaneous melanoma, and Ezh2 inactivation antagonizes metastatic progression in murine melanoma models (Manning et al., 2015; Zingg et al., 2015). Moreover, in several cancers, tumor stemness and EMT have been linked to immune evasion (Hölzel and Tüting, 2016; Lou et al., 2016; Tripathi et al., 2016). Finally, tumor biopsy specimens from cutaneous melanoma patients displaying resistance to checkpoint blockade therapy showed increased expression of melanoma dedifferentiation genes in favor of melanocyte lineage genes (Hugo et al., 2016). Hence, melanoma might similarly take advantage of PRC2 activity to promote EMT, resulting in resistance to immune pressure during T cell-engaging immunotherapy and ultimately metastasis.

Despite some long-term responders, a notable number of melanoma patients are intrinsically resistant to PD-1/PD-L1 checkpoint blockade, for instance due to a paucity of $PD\text{-}1^+$ TILs or of PD-L1 expression on tumor cells (Herbst et al., 2014; Hugo et al., 2016; Tumeh et al., 2014; Van Allen et al., 2015). Since blockade of Ezh2 is associated with downregulation of the PD-1/PD-L1 axis and, therefore, independent of PD-1 and PD-L1 expression levels in patients, the combination therapies presented here might offer an alternative strategy for patients resistant to anti-PD-1 and anti-PD-L1 treatment.

EZH2 inhibitors are currently tested in several clinical trials in solid and hematological malignancies with the aim of exerting an antiproliferative effect on the cancer cells (Kim and Roberts, 2016). Our data suggest that subtoxic doses of EZH2 inhibitors might suffice to prevent cancer immune resistance during immunotherapy. Hence, targeting of EZH2 is an attractive strategy to combine with cancer immunotherapy.

EXPERIMENTAL PROCEDURES

Mice

3-month-old female C57BL/6 mice were purchased from Charles River Laboratories. $Tcrbd^{-/-}$, $Rag1^{-/-}$, $Ifng^{-/-}$, $Tnf^{-/-}$, and $Pmel^{Si}$ $Thy1^{a}$ transgenic mice, all on a C57BL/6 background, were purchased from The Jackson Laboratory. $Tyr::Nras^{Q61K}$ *Cdkn2a* ($p16^{Ink4a}$)-deficient (referred to as $Nras^{Q61K}$ $Ink4a^{-/-}$) transgenic mice on a mixed background were mated, genotyped, and monitored for tumor development as described previously (Zingg et al., 2015). Tumor volume was calculated as described previously (Arenas-Ramirez

Figure 4. Ezh2 Inhibition Combined with Immunotherapy Stimulates $CD8^+$ T Cells and Suppresses the PD-1/PD-L1 Axis

(A–E) Mice harboring B16-F10 melanoma cells were treated as in Figure 3D. Flow cytometry analyses of tumor-infiltrating lymphocytes (TILs) and tumor-draining lymph nodes (TDLNs) (A), with quantification of total cell counts (B, left axes, colored bars), percentages (B, right axes, square points) of indicated immune cell subsets, and corresponding ratios of $CD8^+$ T cells versus $CD4^+$ $CD25^+$ $FoxP3^+$ regulatory T cells (C). CD44, CD62L, and CD69 expression on $CD8^+$ T cells in TILs and TDLNs (D). PD-1 expression on $CD8^+$ T cells by percentages and MFI (red numbers) in TILs and TDLNs (E).

(F and G) Immunofluorescence staining for Pax3, PD-L1, and CD3 in RIM-3 (F) from mice treated as in Figure 3D, and quantification of $Pax3^+$ $PD\text{-}L1^+$ cells in areas poor or rich in $CD3^+$ cells ($CD3^+$ $n < 5$ versus $n > 20$ per field) (G). Scale bars, 50 μm.

(H) Tumor growth kinetics in mice engrafted with RIM-3 cells and receiving PBS, IL-2cx, PD-1-blocking antibody (a-PD-1), or GSK503 as indicated. Black arrows mark the time point when treatment started.

Data are presented as mean ± SEM of n = 4–6 (B and C, TILs), n = 16–17 (B and C, TDLNs), and n = 5 (E–H) from six (A–C), two (D), and five (E) independent experiments or one experiment (G and H). For TILs, samples of mice receiving the same treatment were pooled prior to analysis. p values were calculated using an unpaired Student's t test (B, and percentages in E) or ANOVA and the Fisher's LSD test (G and H). NS, not significant; $^*p < 0.05$; $^{**}p < 0.01$; $^{***}p < 0.001$; $^{****}p < 0.0001$. See also Figures S4 and S5.

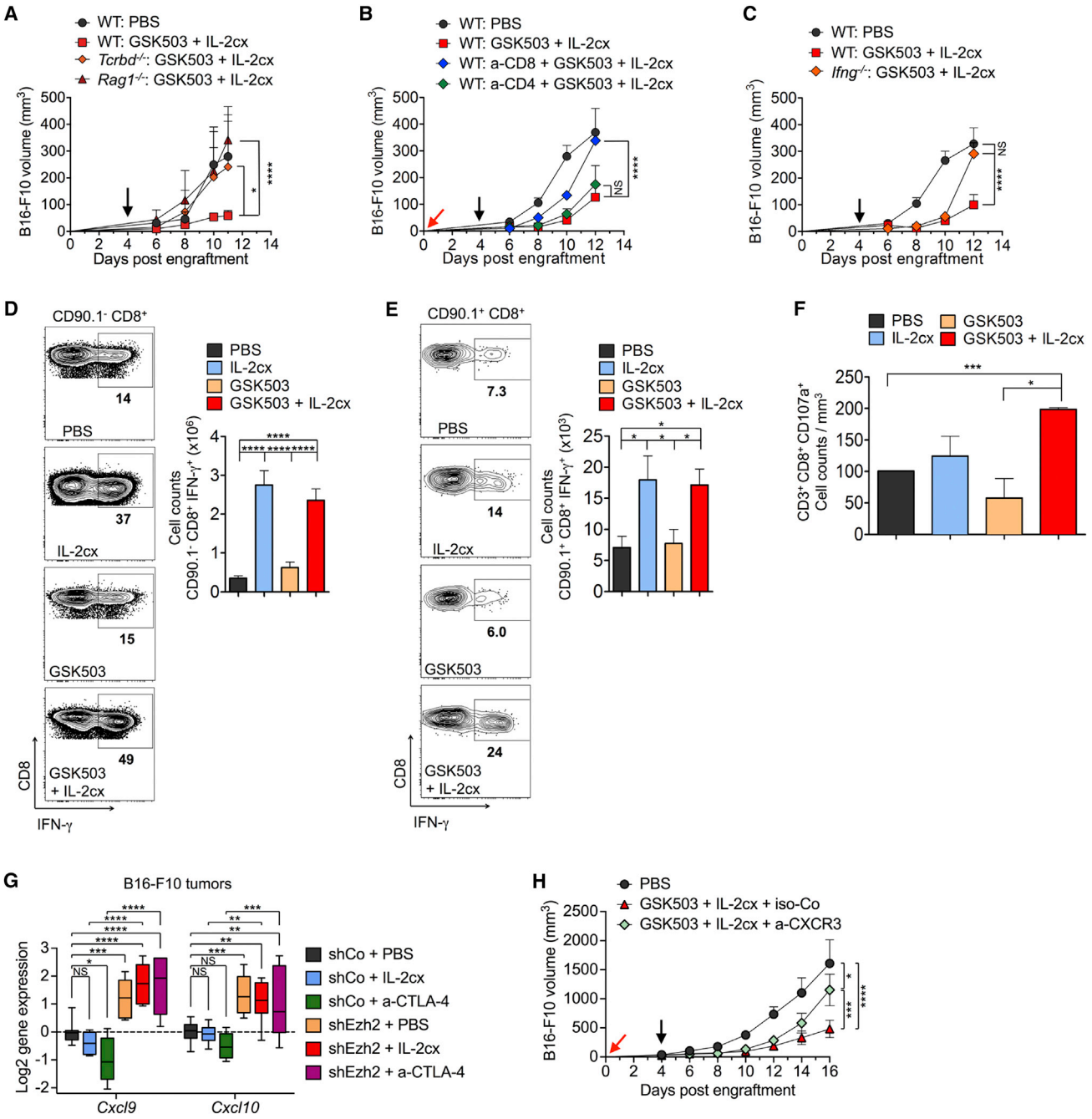

Figure 5. Effects of Combination Therapy Depend on Migrating IFN-γ$^+$ CD8$^+$ T Cells

(A–C) Growth of B16-F10 tumors during PBS versus GSK503 + IL-2cx therapy in WT, *Tcrbd*$^{-/-}$, and *Rag1*$^{-/-}$ mice (A), WT mice depleted of CD4$^+$ or CD8$^+$ T cells using depleting mAbs (B), or *Ifng*$^{-/-}$ mice. (C).

(D and E) Mice were adoptively transferred with CD90.1$^+$ Pmel-specific T cell-receptor-transgenic CD8$^+$ T cells, followed by treatment as in Figure 3D. Shown is IFN-γ production and quantification of IFN-γ$^+$ cells within CD90.1$^-$ polyclonal (D) versus CD90.1$^+$ Pmel-specific (E) CD8$^+$ T cells from TDLNs.

(F) Mice were treated as in Figure 3D, followed by assessment of intratumoral CD107a$^+$ CD8$^+$ T cells per cubic millimeter of tumor.

(G) qRT-PCR for *Cxcl9* and *Cxcl10* in shCo- or shEzh2-transfected B16-F10 melanoma nodules from mice receiving PBS, IL-2cx, or a-CTLA-4.

(H) Tumor growth kinetics in B16-F10-bearing mice receiving PBS, GSK503 + IL-2cx, or GSK503 + IL-2cx plus CXCR3-blocking antibody (a-CXCR3).

Black and red arrows indicate the time point of treatment start and mAb injection, respectively. Data are presented as mean ± SEM of n = 8 (A), n = 6 (B), n = 7–9 (C), n = 8–13 (D), n = 7–13 (E), n = 2 (F), and n = 9 (H) and as median ± 100% range of n = 5–8 (G) from two (A–F and H) and three (G) independent experiments. p values were calculated using ANOVA and Bonferroni correction (A–C and H), the Fisher's LSD test (G), or an unpaired Student's t test (D–F). NS, not significant, *p < 0.05, **p < 0.01, ***p < 0.001, ****p < 0.0001.

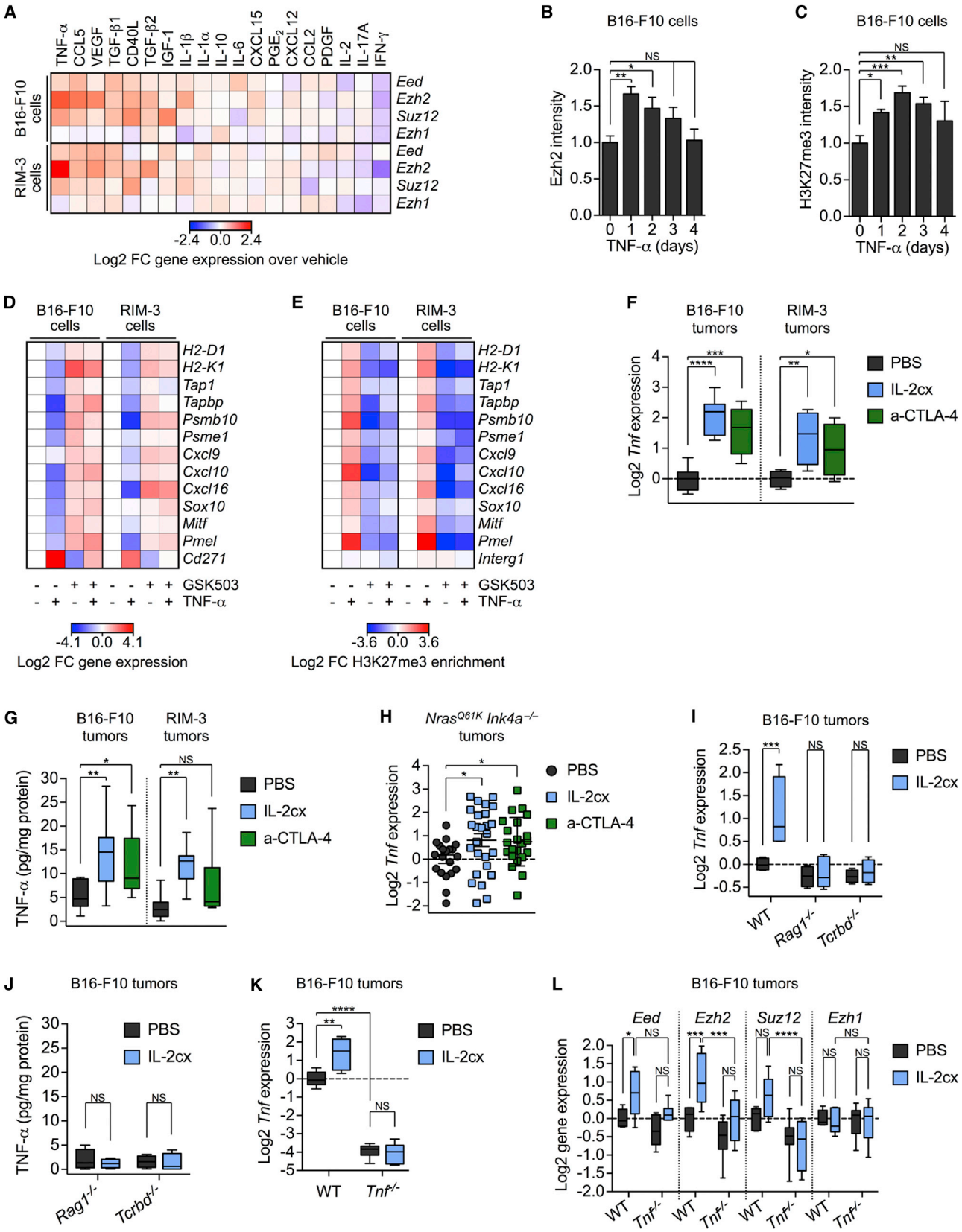

(legend on next page)

et al., 2016). Skin-melanoma-specific survival of *Nras*^{Q61K} *Ink4a*$^{-/-}$ mice was considered melanoma independent (censored event), when at the time point of sacrifice more than 50% of skin melanomas showed a tumor volume reduction greater than 50%. Animal experiments were approved by the veterinary authorities of Canton of Zurich, Switzerland, and were performed in accordance with Swiss law and GlaxoSmithKline policy on the Care, Welfare, and Treatment of Animals. Pre-established exclusion criteria were based on the Canton of Zurich veterinary authority's guidelines and included substantial weight loss of Δm >15% of initial body weight.

Cell Cultures

The murine B16-F10 (CRL-6475, ATCC), LLC1, and MC-38 (provided by R. Schwendener) cell lines were cultured in growth medium. RIM-3 skin melanoma cells derived from a *Nras*^{Q61K} *Ink4a*$^{-/-}$ mouse on a pure C57BL/6 background (Zingg et al., 2015) were cultured on plates coated with fibronectin (F1141, Sigma-Aldrich) using melanocyte medium, which was DMEM/F-12 (21041, Thermo Fisher Scientific) supplemented with 10% fetal calf serum (FCS), penicillin-streptomycin, and 200 nM phorbol 12-myristate 13-acetate (PMA; P1585, Sigma-Aldrich).

Adoptive Tumor Models

Recipient mice were intradermally or subcutaneously engrafted with either 500,000 RIM-3 cells or 1 × 10^6 B16-F10, LLC1, or MC-38 cells. Mice were sacrificed either at indicated time points or upon reaching a maximal tumor volume of V = 2,000 mm^3.

In Vivo Treatments

Recombinant human IL-2 (Teceleukin, Roche), anti-CTLA-4 mAb (a-CTLA-4, 9D9, BioXcell), anti-PD-1 mAb (a-PD-1, RMP1-14, BioXcell), anti-CXCR-3 (a-CXCR-3, CXCR3-173, BioXcell), isotype control (iso-Co, C1.18.4, BioXcell), and GSK503 (GlaxoSmithKline) were purchased. IL-2cx was prepared by mixing IL-2 and anti-IL-2 mAb NARA1 as described previously (Arenas-Ramirez et al., 2016). GSK503 was diluted (15 mg/mL) in 20% Captisol solution (Ligand Pharmaceuticals). Treatment of B16-F10-engrafted mice began when tumors became visible (at approximately day 4). Treatment of RIM-3-engrafted mice was initiated when tumors reached a size of V > 150 mm^3 (at about 20 days). Treatment of *Nras*^{Q61K} *Ink4a*$^{-/-}$ mice was started when at least one skin melanoma reached a diameter of >2 mm (at about 5–7 months). Ezh2 inhibition was achieved by daily intraperitoneal (i.p.) injection of 150 mg/kg GSK503 for B16-F10 and RIM-3 and 75 mg/kg GSK503 for LLC1 and MC-38 until termination of the experiment. Where indicated, mice harboring B16-F10 received i.p. injections of IL-2cx (1.5 μg hIL-2/15 μg NARA1), or 250 μg a-CTLA-4 for 4 consecutive days, while LLC1 or MC-38-bearing animals received three weekly cycles consisting of IL-2cx (1.0 μg hIL-2/10 μg NARA1) injections for 4 consecutive days. Mice bearing RIM-3 received i.p. injections of IL-2cx (1.5 μg hIL-2/15 μg NARA1) or 250 μg a-PD-1 every other day until termination of the experiment. For *Nras*^{Q61K} *Ink4a*$^{-/-}$ mice, 150 mg/kg GSK503 and, where indicated, IL-2cx (1.0 μg hIL-2/10 μg NARA1) or 167 μg a-CTLA-4 was applied i.p. three times a week until termination of the experiment. Where mentioned, depletion of CD4$^+$ cells was performed using 250 μg anti-CD4 mAb (a-CD4, clone GK1.5, BioXcell), CD8$^+$ cells using 500 μg anti-CD8 mAb (a-CD8, clone YTS169, BioXcell), and CXCR3 using 500 μg a-CXCR3 mAb. Depleting mAbs were administered i.p. every other day (a-CD4 and a-CD8) or every 3 days (a-CXCR3) starting on day 0 of tumor implantation until the end of the experiment. Where indicated, CD90.1$^+$ Pmel-specific CD8$^+$ T cells were obtained as established previously (Arenas-Ramirez et al., 2016) from *Pmel*^{Si} *Thy1*^{a} transgenic mice. At least 2 × 10^6 purified and carboxyfluorescein succinimidyl ester (CFSE; Thermo Fisher Scientific)-labeled CD8$^+$ T cells were adoptively transferred to recipients. Cell proliferation was measured using bromodeoxyuridine (BrdU; B5002, Sigma-Aldrich) as described previously (Arenas-Ramirez et al., 2016).

Flow Cytometry

Single-cell suspensions of lymph nodes, spleen, and tumors were prepared and stained as previously described (Arenas-Ramirez et al., 2016). Fluorochrome-conjugated antibodies are listed in Table S1. Intracellular CD107a, FoxP3, and IFN-γ staining was performed following the manufacturers' instructions after in vitro restimulation using PMA and ionomycin (0.1 mg/mL and 1 mg/mL, P8139 and I0634, Sigma-Aldrich) in the presence of brefeldin A and monensin (2 mg/mL, B7651 and M5273, Sigma-Aldrich). Samples were acquired with a BD LSR II flow cytometer (BD Biosciences) and analyzed using FlowJo software.

Histological Analysis and Immunofluorescence

For immunofluorescence staining, mouse tumor samples were processed and stained as established (O'Connell et al., 2013; Zingg et al., 2015) using primary and secondary antibodies (Tables S2 and S3). Sections were recorded using a DMI 6000B microscope (Leica). Images were processed by Photoshop CS5 software (Adobe) to exclude areas covered by CD45 or CD3 staining. To measure cytoplasmic Pmel labeling, brightness of the Pmel signal was measured with CellProfiler software (Carpenter et al., 2006) (MeasureImageIntensity). To measure nuclear staining (Ezh2, Mitf, Zeb1), algorithms in CellProfiler identifying nuclei (IdentifyPrimaryObjects) and quantifying nuclear intensities (MeasureObjectIntensity) were applied. CD45$^+$ or Pax3$^+$ PD-L1$^+$ cells were counted manually. For each tumor, at least ten fields containing either n < 5 or n > 20 CD45$^+$ or CD3$^+$ cells were quantified.

In Vitro Silencing and Inhibition of Ezh2

To stably silence *Ezh2*, B16-F10 cells were transfected with small hairpin RNA (shRNA)-expressing plasmids encoding either a scrambled shRNA (shCo; SHC002, Sigma-Aldrich) or Ezh2 mRNA-targeting shRNA (shEzh2; TRCN0000039040, Sigma-Aldrich). 10 μg plasmid was applied in combination with jetPEI DNA Transfection Reagent (101-10N, Polyplus Transfection) according to the manufacturer's recommendations. Transfected cells were selected using 1 μg/mL puromycin (A11138-02, Life Technologies) for 1 week before further assessment. To pharmacologically inhibit Ezh2, cells were treated with 1 μM GSK503 for 8 days before further assessment. Efficiency of shEzh2 and GSK503 has been validated previously (Zingg et al., 2015).

In Vitro Growth Factor and Chemokine Treatments

Growth factors and chemokines indicated in Table S4 were resolved in 0.1% BSA in PBS. Cells were grown in starvation medium (1% FCS) for 48 hr and subsequently treated with growth factors and chemokines, 1000 U/mL

Figure 6. TNF-α-Producing T Cells Cause Loss of Melanoma Immunogenicity

(A) qRT-PCR for PRC2 genes in B16-F10 and RIM-3 cells after 48 hr incubation with indicated soluble factors. Heatmap shows Log2 FC values relative to vehicle.
(B and C) Quantification of western blots (Figure S6A) for Ezh2 (B) and H3K27me3 (C) in B16-F10 cells after incubation with TNF-α.
(D and E) qRT-PCR for selected genes (D) and ChIP for H3K27me3 and subsequent qPCR in promoter regions of selected loci (E) in B16-F10 and RIM-3 cells after GSK503-mediated Ezh2 blockade and 48-hr TNF-α stimulation. Heatmap shows Log2 FC values relative to vehicle.
(F and G) qRT-PCR (F) and ELISA (G) for *Tnf*/TNF-α in B16-F10 melanoma from mice receiving PBS, IL-2cx, or a-CTLA-4.
(H) qRT-PCR for *Tnf* on *Nras*^{Q61K} *Ink4a*$^{-/-}$ melanomas from mice receiving PBS, IL-2cx, or a-CTLA-4.
(I and J) qRT-PCR (I) and ELISA (J) for *Tnf*/TNF-α in B16-F10 melanoma nodules from WT, *Rag1*$^{-/-}$, or *Tcrbd*$^{-/-}$ mice receiving PBS or IL-2cx.
(K and L) qRT-PCR for *Tnf* (K) and PRC2 genes (L) in B16-F10 melanoma nodules from WT or *Tnf*$^{-/-}$ mice receiving PBS or IL-2cx.
Data are presented as mean of n = 3 (A, D, and E), mean ± SEM of n = 3 (B and C), n = 20 tumors of eight mice (H, PBS), n = 26 tumors of nine mice (H, IL-2cx), and n = 22 tumors of ten mice (H, a-CTLA-4) and median ± 100% range of n = 5–8 (F, B16-F10, K, and L), n = 4 (F, RIM-3, I, and J), n = 9 (G, B16-F10), and n = 7 (G, RIM-3) from three (A–G), one (H), or two (I–L) independent experiments. p values were calculated using ANOVA and the Fisher's LSD test. NS, not significant, *p < 0.05, **p < 0.01, ***p < 0.001, ****p < 0.0001. See also Figure S6.

IL-2cx or 16.7 mg/mL a-CTLA-4 for 48 hr in starvation medium before further assessment.

RNA Isolation and qRT-PCR

Cultured cells were lysed in Buffer RLT (79216, QIAGEN) containing 1% 2-mercaptoethanol, while tumor nodules were homogenized in the same buffer using a Polytron PT 2100 tissue disperser (Kinematica). Subsequent RNA extraction and DNase treatment of samples was performed using the RNeasy Mini Kit (74104, QIAGEN) and RNase-Free DNase Set (79254, QIAGEN) according to manufacturer's guidelines. Purified RNA was subjected to reverse transcriptase (RT) reaction using the Maxima First Strand cDNA Synthesis Kit (K1641, Thermo Fisher Scientific) followed by an RNase H (EN0202, Thermo Fisher Scientific) digestion step according to the manufacturer's recommendations. Real-time qPCR (qPCR) was performed on a LightCycler 480 System (Roche) using LightCycler 480 SYBR Green I Master (4707516001, Roche). qRT-PCR primers are listed in Table S5. Relative quantified RNA was normalized using *Usf1* as housekeeping transcript.

Chromatin Isolation and ChIP

Chromatin isolation and ChIP of cultured cells and tumor nodules was performed according to the manufacturer's guidelines using the SimpleChIP Plus Enzymatic Chromatin IP Kit (9005, Cell Signaling Technology). Briefly, 10^7 cultured cells were crosslinked on culture plates and subjected to chromatin isolation, while tumor samples of 150 mg were minced using scissors prior to crosslinking. Crosslinked samples were disaggregated into single cells using a Polytron PT 2100 tissue disperser. Isolated nuclei were digested with 5 μL micrococcal nuclease for 30 min at 37°C, and nuclei were lysed using a SONOPULS HD 2070 Ultrasonic Homogenizer (Bandelin). ChIP was performed with 18 μg chromatin and the primary antibodies listed in Table S2. qPCR was performed on a LightCycler 480 System using the KAPA SYBR Fast qPCR Kit Master Mix (KR0389, KAPA Biosystems). Primers were specified to amplify genomic DNA from a region flanking the transcriptional starting site −500 bp to +100 bp devoid of local CpG islands, and are indicated in Table S6. Relative promoter enrichment was normalized to chromatin inputs, and the intergenic region 1 (*Interg1*) was used as negative control.

Protein Isolation and Western Blotting

Protein lysates of cultured cells and tumor nodules were isolated and western blots performed as described previously (Zingg et al., 2015). Briefly, SDS-PAGE was carried out on 4%–20% Mini-PROTEAN TGX Gels (456-1094, Bio-Rad). Primary antibodies (Table S2) were applied in Odyssey blocking buffer (927-40000, LI-COR Biosciences) overnight at 4°C and visualized using secondary antibodies (Table S3) in Odyssey blocking buffer for 45 min at room temperature. Blots were scanned and quantified with an Odyssey imaging system (LI-COR Biosciences). Quantified band intensities were normalized using either β-actin or histone 3 as housekeeping protein.

ELISA

4 mg/mL protein lysate isolated as for western blotting was subjected to the Mouse TNF-alpha Quantikine ELISA Kit (MTA00B, R&D Systems) according to the manufacturer's protocol. Optical density was measured using a DTX 880 Multimode Detector (Beckman Coulter) at 450 nm.

Gene Expression Correlation Analyses

The RNA-seq dataset for SKCM was downloaded from TCGA data portal (Cancer Genome Atlas Network, 2015). RSEM normalized RNA-seq reads were used for differential RNA expression analysis using R software. Genes indicative of presence of intratumoral $CD8^+$ T cells have previously been defined (Bindea et al., 2013). Within the TCGA-SKCM RNA-seq dataset, expression of each of these $CD8^+$ T cell signature genes was correlated to the expression of epigenetic modifier genes. Significance of correlative gene expression was calculated by using Pearson's product-moment correlation coefficient (*r*).

Statistical Analyses

Statistical analyses were performed in GraphPad Prism 6. p values were calculated with a two-sided unpaired Student's t test or, for comparison of more than two groups, ANOVA and Fisher's least significant difference (LSD) or Bonferroni correction. p values for comparison of Kaplan-Meier curves were calculated with the log-rank (Mantel-Cox) test. The expected variance was similar between groups. For all analyses, significance was accepted at a 95% confidence level ($p < 0.05$).

SUPPLEMENTAL INFORMATION

Supplemental Information includes six figures and six tables and can be found with this article online at http://dx.doi.org/10.1016/j.celrep.2017.07.007.

AUTHOR CONTRIBUTIONS

D.Z., N.A.-R., L.S., and O.B. designed the experiments. D.Z., N.A.-R., D.S., R.A.R., A.T.A., and J.H. performed the experiments. D.Z., N.A.-R., L.S., and O.B. analyzed the data. D.Z., N.A.-R., L.S., and O.B. wrote the manuscript.

ACKNOWLEDGMENTS

We thank J. Debbache, S. Schaefer, E. Tuncer, and S. Varum for support with transgenic mice and E. Ammann and A. Klug for help with experiments. We thank P. Cheng (University Hospital Zurich) for assistance in generating TCGA gene correlations. We thank G. Christofori (University of Basel) for providing shEzh2-expressing plasmid, M. T. McCabe and C. L. Creasy (GlaxoSmithKline) for providing GSK503, and H. Arnheiter (National Institutes of Health) for providing Mitf antibody. This work was funded by Swiss National Science Foundation grants PP00P3-128421, CRSII3-136203, PP00P3-150751 (O.B.), and S-41003-04-01(L.S.); Swiss Cancer Research grants KFS-3375-02-2014 (O.B.) and KFS-2897-02-2012 (L.S.); the Zurich University Research Priority Program "Translational Cancer Research"; and the Helmut Horten Foundation (L.S. and O.B.).

Received: May 4, 2016
Revised: May 24, 2017
Accepted: July 5, 2017
Published: July 25, 2017

REFERENCES

Arenas-Ramirez, N., Woytschak, J., and Boyman, O. (2015). Interleukin-2: biology, design and application. Trends Immunol. *36*, 763–777.

Arenas-Ramirez, N., Zou, C., Popp, S., Zingg, D., Brannetti, B., Wirth, E., Calzascia, T., Kovarik, J., Sommer, L., Zenke, G., et al. (2016). Improved cancer immunotherapy by a CD25-mimobody conferring selectivity to human interleukin-2. Sci. Transl. Med. *8*, 367ra166.

Béguelin, W., Popovic, R., Teater, M., Jiang, Y., Bunting, K.L., Rosen, M., Shen, H., Yang, S.N., Wang, L., Ezponda, T., et al. (2013). EZH2 is required for germinal center formation and somatic EZH2 mutations promote lymphoid transformation. Cancer Cell *23*, 677–692.

Bindea, G., Mlecnik, B., Tosolini, M., Kirilovsky, A., Waldner, M., Obenauf, A.C., Angell, H., Fredriksen, T., Lafontaine, L., Berger, A., et al. (2013). Spatiotemporal dynamics of intratumoral immune cells reveal the immune landscape in human cancer. Immunity *39*, 782–795.

Boyman, O., Kovar, M., Rubinstein, M.P., Surh, C.D., and Sprent, J. (2006). Selective stimulation of T cell subsets with antibody-cytokine immune complexes. Science *311*, 1924–1927.

Cancer Genome Atlas Network (2015). Genomic classification of cutaneous melanoma. Cell *161*, 1681–1696.

Caramel, J., Papadogeorgakis, E., Hill, L., Browne, G.J., Richard, G., Wierinckx, A., Saldanha, G., Osborne, J., Hutchinson, P., Tse, G., et al. (2013). A switch in the expression of embryonic EMT-inducers drives the development of malignant melanoma. Cancer Cell *24*, 466–480.

Carpenter, A.E., Jones, T.R., Lamprecht, M.R., Clarke, C., Kang, I.H., Friman, O., Guertin, D.A., Chang, J.H., Lindquist, R.A., Moffat, J., et al. (2006). CellProfiler: image analysis software for identifying and quantifying cell phenotypes. Genome Biol. *7*, R100.

Chen, L., Gibbons, D.L., Goswami, S., Cortez, M.A., Ahn, Y.H., Byers, L.A., Zhang, X., Yi, X., Dwyer, D., Lin, W., et al. (2014). Metastasis is regulated via microRNA-200/ZEB1 axis control of tumour cell PD-L1 expression and intratumoral immunosuppression. Nat. Commun. *5*, 5241.

Denecker, G., Vandamme, N., Akay, O., Koludrovic, D., Taminau, J., Lemeire, K., Gheldof, A., De Craene, B., Van Gele, M., Brochez, L., et al. (2014). Identification of a ZEB2-MITF-ZEB1 transcriptional network that controls melanogenesis and melanoma progression. Cell Death Differ. *21*, 1250–1261.

DuPage, M., Chopra, G., Quiros, J., Rosenthal, W.L., Morar, M.M., Holohan, D., Zhang, R., Turka, L., Marson, A., and Bluestone, J.A. (2015). The chromatin-modifying enzyme Ezh2 is critical for the maintenance of regulatory T cell identity after activation. Immunity *42*, 227–238.

Herbst, R.S., Soria, J.C., Kowanetz, M., Fine, G.D., Hamid, O., Gordon, M.S., Sosman, J.A., McDermott, D.F., Powderly, J.D., Gettinger, S.N., et al. (2014). Predictive correlates of response to the anti-PD-L1 antibody MPDL3280A in cancer patients. Nature *515*, 563–567.

Hölzel, M., and Tüting, T. (2016). Inflammation-induced plasticity in melanoma therapy and metastasis. Trends Immunol. *37*, 364–374.

Hugo, W., Zaretsky, J.M., Sun, L., Song, C., Moreno, B.H., Hu-Lieskovan, S., Berent-Maoz, B., Pang, J., Chmielowski, B., Cherry, G., et al. (2016). Genomic and transcriptomic features of response to anti-PD-1 therapy in metastatic melanoma. Cell *165*, 35–44.

Kim, K.H., and Roberts, C.W.M. (2016). Targeting EZH2 in cancer. Nat. Med. *22*, 128–134.

Krieg, C., Létourneau, S., Pantaleo, G., and Boyman, O. (2010). Improved IL-2 immunotherapy by selective stimulation of IL-2 receptors on lymphocytes and endothelial cells. Proc. Natl. Acad. Sci. USA *107*, 11906–11911.

Larkin, J., Chiarion-Sileni, V., Gonzalez, R., Grob, J.J., Cowey, C.L., Lao, C.D., Schadendorf, D., Dummer, R., Smylie, M., Rutkowski, P., et al. (2015). Combined nivolumab and ipilimumab or monotherapy in untreated melanoma. N. Engl. J. Med. *373*, 23–34.

Levin, A.M., Bates, D.L., Ring, A.M., Krieg, C., Lin, J.T., Su, L., Moraga, I., Raeber, M.E., Bowman, G.R., Novick, P., et al. (2012). Exploiting a natural conformational switch to engineer an interleukin-2 'superkine'. Nature *484*, 529–533.

Lou, Y., Diao, L., Cuentas, E.R., Denning, W.L., Chen, L., Fan, Y.H., Byers, L.A., Wang, J., Papadimitrakopoulou, V.A., Behrens, C., et al. (2016). Epithelial-mesenchymal transition is associated with a distinct tumor microenvironment including elevation of inflammatory signals and multiple immune checkpoints in lung adenocarcinoma. Clin. Cancer Res. *22*, 3630–3642.

Manning, C.S., Hooper, S., and Sahai, E.A. (2015). Intravital imaging of SRF and Notch signalling identifies a key role for EZH2 in invasive melanoma cells. Oncogene *34*, 4320–4332.

Nagarsheth, N., Peng, D., Kryczek, I., Wu, K., Li, W., Zhao, E., Zhao, L., Wei, S., Frankel, T., Vatan, L., et al. (2016). PRC2 epigenetically silences Th1-type chemokines to suppress effector T-cell trafficking in colon cancer. Cancer Res. *76*, 275–282.

O'Connell, M.P., Marchbank, K., Webster, M.R., Valiga, A.A., Kaur, A., Vultur, A., Li, L., Herlyn, M., Villanueva, J., Liu, Q., et al. (2013). Hypoxia induces phenotypic plasticity and therapy resistance in melanoma via the tyrosine kinase receptors ROR1 and ROR2. Cancer Discov. *3*, 1378–1393.

Peng, D., Kryczek, I., Nagarsheth, N., Zhao, L., Wei, S., Wang, W., Sun, Y., Zhao, E., Vatan, L., Szeliga, W., et al. (2015). Epigenetic silencing of TH1-type chemokines shapes tumour immunity and immunotherapy. Nature *527*, 249–253.

Rosenberg, S.A. (2014). IL-2: the first effective immunotherapy for human cancer. J. Immunol. *192*, 5451–5458.

Schreiber, R.D., Old, L.J., and Smyth, M.J. (2011). Cancer immunoediting: integrating immunity's roles in cancer suppression and promotion. Science *331*, 1565–1570.

Shakhova, O., Zingg, D., Schaefer, S.M., Hari, L., Civenni, G., Blunschi, J., Claudinot, S., Okoniewski, M., Beermann, F., Mihic-Probst, D., et al. (2012). Sox10 promotes the formation and maintenance of giant congenital naevi and melanoma. Nat. Cell Biol. *14*, 882–890.

Spranger, S., Spaapen, R.M., Zha, Y., Williams, J., Meng, Y., Ha, T.T., and Gajewski, T.F. (2013). Up-regulation of PD-L1, IDO, and T(regs) in the melanoma tumor microenvironment is driven by CD8(+) T cells. Sci. Transl. Med. *5*, 200ra116.

Topalian, S.L., Drake, C.G., and Pardoll, D.M. (2015). Immune checkpoint blockade: a common denominator approach to cancer therapy. Cancer Cell *27*, 450–461.

Tripathi, S.C., Peters, H.L., Taguchi, A., Katayama, H., Wang, H., Momin, A., Jolly, M.K., Celiktas, M., Rodriguez-Canales, J., Liu, H., et al. (2016). Immunoproteasome deficiency is a feature of non-small cell lung cancer with a mesenchymal phenotype and is associated with a poor outcome. Proc. Natl. Acad. Sci. USA *113*, E1555–E1564.

Tumeh, P.C., Harview, C.L., Yearley, J.H., Shintaku, I.P., Taylor, E.J., Robert, L., Chmielowski, B., Spasic, M., Henry, G., Ciobanu, V., et al. (2014). PD-1 blockade induces responses by inhibiting adaptive immune resistance. Nature *515*, 568–571.

Ueha, S., Yokochi, S., Ishiwata, Y., Ogiwara, H., Chand, K., Nakajima, T., Hachiga, K., Shichino, S., Terashima, Y., Toda, E., et al. (2015). Robust antitumor effects of combined anti-CD4-depleting antibody and anti-PD-1/PD-L1 immune checkpoint antibody treatment in mice. Cancer Immunol. Res. *3*, 631–640.

Van Allen, E.M., Miao, D., Schilling, B., Shukla, S.A., Blank, C., Zimmer, L., Sucker, A., Hillen, U., Geukes Foppen, M.H., Goldinger, S.M., et al. (2015). Genomic correlates of response to CTLA-4 blockade in metastatic melanoma. Science *350*, 207–211.

Wang, X., He, X., Zhao, F., Wang, J., Zhang, H., Shi, F., Zhang, Y., Cai, K., and Dou, J. (2014). Regulation gene expression of miR200c and ZEB1 positively enhances effect of tumor vaccine B16F10/GPI-IL-21 on inhibition of melanoma growth and metastasis. J. Transl. Med. *12*, 68.

Wherry, E.J., and Kurachi, M. (2015). Molecular and cellular insights into T cell exhaustion. Nat. Rev. Immunol. *15*, 486–499.

Zhao, E., Maj, T., Kryczek, I., Li, W., Wu, K., Zhao, L., Wei, S., Crespo, J., Wan, S., Vatan, L., et al. (2016). Cancer mediates effector T cell dysfunction by targeting microRNAs and EZH2 via glycolysis restriction. Nat. Immunol. *17*, 95–103.

Zingg, D., Debbache, J., Schaefer, S.M., Tuncer, E., Frommel, S.C., Cheng, P., Arenas-Ramirez, N., Haeusel, J., Zhang, Y., Bonalli, M., et al. (2015). The epigenetic modifier EZH2 controls melanoma growth and metastasis through silencing of distinct tumour suppressors. Nat. Commun. *6*, 6051.